Front. Energy 2017, 11(4): 437–451
https://doi.org/10.1007/s11708-017-0509-z

REVIEW ARTICLE

Sanli TANG, Jie SUN, Hui HONG, Qibin LIU

Solar fuel from photo-thermal catalytic reactions with spectrum-selectivity: a review

Abstract Solar fuel is one of the ideal energy sources in the future. The synergy of photo and thermal effects leads to a new approach to higher solar fuel production under relatively mild conditions. This paper reviews different approaches for solar fuel production from spectrum-selective photo-thermal synergetic catalysis. The review begins with the meaning of synergetic effects, and the mechanisms of spectrum-selectivity and photo-thermal catalysis. Then, from a technical perspective, a number of experimental or theoretical works are sorted by the chemical reactions and the sacrificial reagents applied. In addition, these works are summarized and tabulated based on the operating conditions, spectrum-selectivity, materials, and productivity. A discussion is finally presented concerning future development of photo-thermal catalytic reactions with spectrum-selectivity.

Keywords photo-thermal catalysis, spectrum-selectivity, solar fuel, full-spectrum

1 Introduction

Energy crisis and growing environmental concerns have raised interests toward the utilization of renewable energy. Solar energy is one of the ideal renewable sources for electricity and fuels in the future. Compared to electricity, solar fuels are of high energy density and easier to store and transport. There are generally two ways to produce solar fuels: by solar thermocatalytic reactions and by solar photocatalytic reactions. To conduct solar thermocatalytic reactions for mass-production of fuels, high temperature or other specific conditions are needed, which requires costly solar concentrators and mirror fields. On the other hand, most photocatalytic reactions operate in relatively mild conditions. However, the fuel production rate is limited. As a result, researchers have come up with photo-thermal catalysis to achieve a complement of the two approaches to utilize their synergetic effects.

Photo-thermalcatalysis is interpreted as the integration of the thermal acceleration of photocatalytic reaction and photo enhancement of thermocatalytic reactions. In thermal acceleration of photocatalytic reaction, the visible and most of infrared parts of solar spectrum may be ineligible for excitation of hole/electrons. However, their thermal effect could be utilized in photocatalysis. In photo enhancement of thermocatalytic reactions, the light-assisted thermocatalysis often operates at a lower temperature and pressure than their heat-driven counterparts.

Research on thermal acceleration of photocatalysis began in 1980s with oxidative degradation of a variety of organics, such as formic acid, isopropanol [1], phenol [2], methyl orange [3], acetone [4], and ammonia [5], over TiO_2 photocatalysts. Besides, temperature dependence of photocatalytic hydrogen production was experimentally investigated, such as the dehydrogenation of various alcohols over Pt/TiO_2 [6], the hydrogen production from methanol-water mixtures over Rh/TiO_2 [7], and the water splitting over $Pt\text{-}RuO_2/TiO_2$ [8]. Localized heat generated from infrared light by carbon nanodots on TiO_2 nanotube increased the rate of pollutant decomposition to 1.5 times [9]. The heat from infrared light was also found to double the activity of Pt/TiO_2 in 10 vol% methanol aqueous solution [10]. Plasmonic heating was utilized to benefit carbonic anhydrase driven photocatalytic hydrogen generation in CO_2 saturated water [11]. The photo and thermal chemical effects of a state-of-art photo-thermal catalyst, Au/TiO_2, was summarized [12]. Surface chemical properties such as reactant adsorption, plasmon resonance (LSPR), and interactions of Au/TiO_2 interface was discussed in detail.

The term "photo-assisted" was coined in a report on thermal decomposition of methanol and isopropanol under

Received May 27, 2017; accepted Sep. 9, 2017; online Nov. 28, 2017

Sanli TANG, Jie SUN (✉), Hui HONG, Qibin LIU
Institute of Engineering Thermophysics, Chinese Academy of Sciences, Beijing 100190, China; University of Chinese Academy of Sciences, Beijing 100049, China
E-mail: sunjie@iet.cn

high-flux irradiation from a Xenon lamp [13]. Effects of light in thermal processes were used in Fischer-Tropsch synthesis [14], decomposition of pollutants [15], purification of exhaust gas [16], etc. For example, thermal decomposition of methanol was known to occur at 200°C–300°C, which occurred at 35°C–60°C over Ti/TiO_2 photo-thermal synergetic catalysis [17]. Under irradiation, Ru loaded layered double hydroxides was heated to 50°C–350°C, where CO_2 reduction was accelerated at elevated temperature [18]. From the perspective of reaction mechanism, thermal catalytic reduction of CO_2 into fuel was reviewed and compared with photo reduction [19] for their combinations. The above content points out that photo-thermal catalysis is a synergy of both thermal and photo effects.

Spectrum-selectivity exists in a variety of materials from Cathedral glasses to heat transfer oil. In solar energy systems, spectrum splitters, in another word, filters, are applied to optimize efficiency in individual wavelength regions. For example, optical filters with selective coating splits lights with a wavelength of 800–1100 nm to PV arrays while others to power cycle. Though spectrum splitting has been regarded to be a promising technology for all-spectrum sunlight harvesting, the optical losses caused by reflection and absorption cannot be retrieved in traditional filters. To reduce these losses, volumetrically-absorptive spectrum splitters are proposed, such as semiconductor-doped glass, ethylene glycol, heat transfer oil, and a variety of nanofluids. Photocatalyst is also spectrum-selective due to its semiconductor nature. If properly designed, the photo-thermal catalysis system may work as spectrum filters with a high fuel-production efficiency, which is called photo-thermal catalytic reactions with spectrum-selectivity (see Fig. 1).

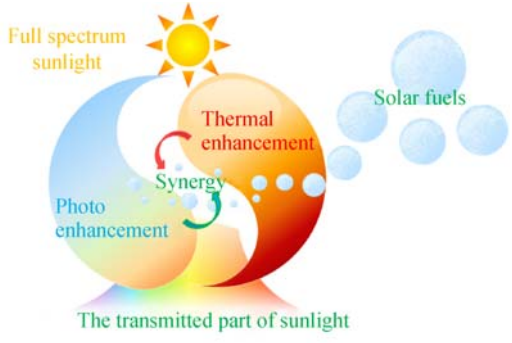

Fig. 1 Photo-thermal catalytic reactions with spectrum-selectivity

This review is focused on photo-thermal catalytic reactions with spectrum-selectivity. The structure is based on the progress in spectrum-selectivity of photocatalysis. To begin with, the basic mechanisms of optical properties and photo-thermal catalysis are introduced. Then, observations of photo-thermal catalysis are listed and explained. Next, a summary of experimental researches is given. And finally, the challenges and potential applications are discussed.

Unlike reviews in material or chemical sciences, this review focuses on the technical applications of photo-thermalcatalysis. Therefore, the works reviewed are organized by the reaction type.

2 Mechanisms of photo-thermal catalytic reactions with spectrum-selectivity

2.1 Mechanism of spectrum-selectivity

Photocatalysts are mostly semiconductor metal oxides. When irradiated, semiconductor generates electrons and holes on the surface, where reactants adsorbed are reduced or oxidized to form products. In this process, light energy was absorbed and stored as chemical energy in the products. The absorption edge is the threshold for eligible light to be used in photocatalysis [20]. It determines the longest wavelength of light that a certain semiconductor accepts. For example, TiO_2 absorbs light with a wavelength shorter than 413.3 nm while CdS has an absorption edge of 729.4 nm. Doping or defects may expand the absorption spectrum to visible region, such as WO_3 [21], TiO_2 [22], and CeO_2 [23].

Another way of spectrum-selectivity is localized surface plasmon resonance (LSPR). The LSPR is light-excited collective oscillation of electron charge in metallic nanoparticles (NPs). Such oscillation causes high absorption of lights with certain wavelengths. Metals, such as Au, Ag, Pt, and Pd, have absorption peaks within the visible range and steep absorption edges. During the preparation of photocatalysts, LSPR effect can be controlled by altering the material and morphology of metallic NPs. Such characteristics provide convenience in design and applications of spectrum-selective photocatalysts.

In LSPR effect, the local electromagnetic field in the vicinity of the particle surface is amplified by electronic charge oscillation. This strong field activates semiconductor catalysts by facilitating transportation of charge carriers [24]. Moreover, metal NPs are also co-catalysts in a wide variety of reactions.

Plasmonic heating from LSPR also enhances the reaction when the illumination intensity is sufficiently high (2.5×10^5 W/m^2 at 532 nm [25]). However, due to heat dissipation, this enhancement is barely observable in common solar concentrators.

Reactants also have spectrum-selectivity and can be utilized to absorb the visible and infrared (Vis-IR) lights that can hardly excite carriers in photocatalysts. It is reported that Vis-IR light is absorbed by water, CO_2, ethylene glycol, propylene glycol, and various oils [26]. The light absorbed provides heat source for photo-thermal catalysis instead of being dissipated in normal photocatalysis.

2.2 Optical property of reaction system

In a photo-thermal catalytic reaction, the catalyst bed is either fluidized or fixed. The fluidized bed is the nanocatalysts suspended in a nanofluid containing certain reactants. The fixed bed is fabricated by depositing nanocatalysts onto solid supports. Theories or simulation methods for the optical property of one nanoparticle include the Mie theory, DDA and FDTD methods. The Mie theory provides the analytical solutions of absorption, scattering and extinction cross sections for a nanosphere. DDA is an approximation of continuum nanostructure by a finite array of polarizable points. Incident light is expressed as electric field to calculate polarizations at every point, then the absorption can be obtained [27]. Finite difference time domain (FDTD) method is an explicit time marching algorithm to calculate Maxwell's curl equations on discrete spatial grids [28], which takes interparticle coupling into account. Optical property of a nanofluid is calculated from the property of one particle and the base fluid [29]. The results acquired in theories and simulations help to design certain photo thermal catalysts [30].

The experimental method for determining the absorption of nanocatalyst is the Uv-Vis-NIR diffusive reflectance spectroscopy (DRS) test. The samples are nanocatalysts fixed on a solid support (in case of fixed bed) or nanofluids contained in a quartz colorimetric utensil (in case of fluidized bed).The data acquired in the test can be converted into absorption spectrum through Kubelka-Munk function [31].

2.3 Mechanism and models of photo-thermal catalysis

A variety of mechanisms have been reported on the kinetics of photocatalysis. The Mars-Van Krevelen mechanism states that in the thermocatalytic oxidation of molecules adsorbed on a metal oxide catalyst (e.g. CeO_2, MnO_2, TiO_2), the surface of catalyst acts as a redox mediator. The reactant adsorbed is oxidized by the surface oxygen on the metal oxide. Then, the metal oxide reduced (e.g. CeO_{2-x}) is re-oxidized by gaseous oxygen. This redox cycle is accelerated by the photo-thermal synergetic effects [32]. The Eley-Rideal mechanism states that a heterogeneous reaction occurs between strongly chemisorbed atoms and physically adsorbed molecules. The latter is attached on the surface of the catalyst by weak van der Waals forces. The Langmuir-Hinshelwood mechanism, which is widely applied in kinetic and mechanism studies of photo-thermal catalysis, states that the reaction occurs between two reactants adsorbed on the surface [33].

In terms of thermodynamics, the Gibbs free energy is the available energy of an ensemble of thermalized excited states, which exists under the condition of constant temperature and pressure [34]. Hence, the Gibbs free energy determines the maximum thermodynamic driving force for electrons and holes to induce the photocatalytic reactions [35]. However, the theory of thermal effects on photocatalysis remains complicated [36] and optimal operating temperature is usually determined through experiments.

2.4 Photo-thermal catalysis in solar all-spectrum utilization systems

Spectrum-selective photo-thermal catalytic reactions are integrated with PV, ordinary photocatalysis, or power cycles to construct a full-spectrum utilization system of concentrated sunlight. Such integration ensures that each energy conversion process operates at its optimal working spectrum. For example, Si PV cells have the highest efficiency with wavelengths of 700–1100 nm, while most spectra out of this region are dissipated into heat. For full-spectrum usage, a solar water purification and renewable electricity generation (SOLWAT) system was designed [37–39]. It included a hybrid solar receiver consisted of photo-degradation and PV modules. In this system, photo-degradation selectively absorbed UV and IR radiations while transmitting visible light to PV.

Hybrid systems with photo-thermal catalysis, PV, and other techniques are emerging concepts. Assessments of such systems are not yet widely discussed. Zamfirescu and Dincer [40] developed a model of a 500 MW solar tower based on a spectrum splitting system integrating PV arrays, photocatalysis and volumetric absorbent Rankine cycles. A case study was presented for an oil sands exploitation area where sulfurous aqueous wastes and hydrogen demand existed. This study offers instructions because this system is also spectrum-selective and poly-generative, similar to hybrid photo-thermal chemical/PV/other systems.

When it comes to performance comparisons between different poly-generative solar energy systems, solar-to-fuel (STF) efficiency is not globally applicable, because STF efficiency is a criterion for a chemical process, where the only input power is sunlight and the only output power is hydrogen derived from solar-driven water splitting. To provide a unified comparison for the system, the electricity consumed by an electrolysis water-splitting needs to be calculated if identical amount of hydrogen is produced by photocatalysis [41]. As a detailed analysis of significant component, exergy comparisons of hydrogen production methods from renewable energy were summarized [42].

3 Progress in photo-thermal catalytic fuel production

Photocatalytic fuel production normally includes water splitting and CO_2 reduction. High fuel generation efficiency is difficult to achieve in pure water or CO_2 because of the rapid recombination of photo-generated electrons and holes. Remedies are proposed such as noble metal loading, addition of sacrificial reagent, and sensitiza-

tion [43]. Among them, sacrificial reagent works as a hole consumer and enhances electron/hole separation, resulting in a higher quantum efficiency. A wide variety of biofuel or sewage components, such as alcohols, organic acids, alkanes, and organic pollutants, are eligible as sacrificial reagents. To show prospects of photo-thermal catalysis, experiments and observations are classified due to sacrificial reagents used. Remarkable experiments on LSPR effects in photo-thermal catalytic reactions are shown in Sub-section 3.1.

3.1 LSPR effects in photo-thermal catalytic reactions

On photo-thermal catalysis with LSPR effects, the plasmon-assisted catalysis was referred to by Adlemanand coworkers in 2009. They observed that Au NPs in glass microchannel perform steam reforming of methanol under irradiation of 532 nm laser beam [44]. Under an irradiation flux of ~10^8 W/m^2, LSPR heating provides the necessary heat of reaction while the reactant fluids remain under ambient conditions.

The LSPR effects are applied by depositing metals on semiconductor NPs. Christopher et al. [45] synthesized Ag nanocubes (edge length being 60 nm) supported α-Al_2O_3 surface. Due to plasmonic resonance of Ag, the absorption spectrum was expanded beyond 400 nm. It was observed that the reaction rate for ethylene epoxidation at 433 K/2.5 suns was comparable to that at 473 K in dark condition. They continued to increase the selectivity of propylene epoxidation with Cu/TiO_2 catalysts at 200°C, maintaining the reduced state of Cu NPs with LSPR [46].

Oxidation reactions of alcohols are widely used in understanding the mechanisms of photo-thermal catalysis hydrogen production. The mechanisms were examined over Au/TiO_2 film [47] between 100°C and 200°C under UV-Vis irradiation. A strong LSPR absorption of around 550 nm was achieved for the catalyst films, which exhibited blue color in visible light (Fig. 2). They clarified the contributions of plasmonic and band gap excitation effects in photo-thermal catalysis by probing the impact of different excitation wavelengths on the thermal-catalytic activity of Au/TiO_2.

3.2 Alcohols or organic acids as sacrificial reagents

The dependence of reaction rate on temperature from 5°C to 30°C was initially observed in hydrogen production from Rh/TiO_2 catalyzed aqueous alcohol solutions [6], such as methanol, ethanol, 1-propanol, and 2-propanol. Then, the hydrogen yield enhancement between 30°C and 100°C at different partial pressures was observed in methanol-water vapor over Rh/TiO_2 and Pt/TiO_2 photo-catalyst [7].

SiO_2/Ag@TiO_2 nanocomposites synthesized by Gao et al. [48] were designed to produce hydrogen and fresh water from seawater. Due to the LSPR effect and its core-shell structure, this nanoparticle absorbs nearly full-spectrum sunlight. Sacrificial reagents, such as methanol, ethylene glycol, glucose, and glycerol were tested in laboratory conditions. On the other hand, parabolic trough collector (PTC) is the most commercialized equipment to achieve a higher concentration ratio [49,50], which further leads to a higher hydrogen production. A PTC-type reactor was also designed and operated under the sun to demonstrate the feasibility (see Fig. 3).The maximum hydrogen generation rate from simulated seawater-glycerol solution was 13.3 mmol/(g_{cat}·h) at the highest reaction temperature (100°C). The results provide evidence of photo-thermal synergetic mechanisms in natural sunlight.

Song et al. [51] investigated UV LED irradiated non-plasmonic Pt/TiO_2 NPs. The loading of Pt expanded the absorption to visible light region (Fig. 4(a)). Organic sacrificial reagents, such as methanol, trielthanolamne, formic acid, and glucose, were studied at different volume concentrations and 70°C–90°C. At 90°C and with formic acid as sacrificial agent, a 714.3 μmol/(g_{cat}·h) of hydrogen yield was acquired, which was 8.1 or 4.2 times higher than that in photo or thermal conditions, respectively. The performances of photo-thermal catalysis over thermal and photo catalysis are shown in Fig. 4(b). They also further

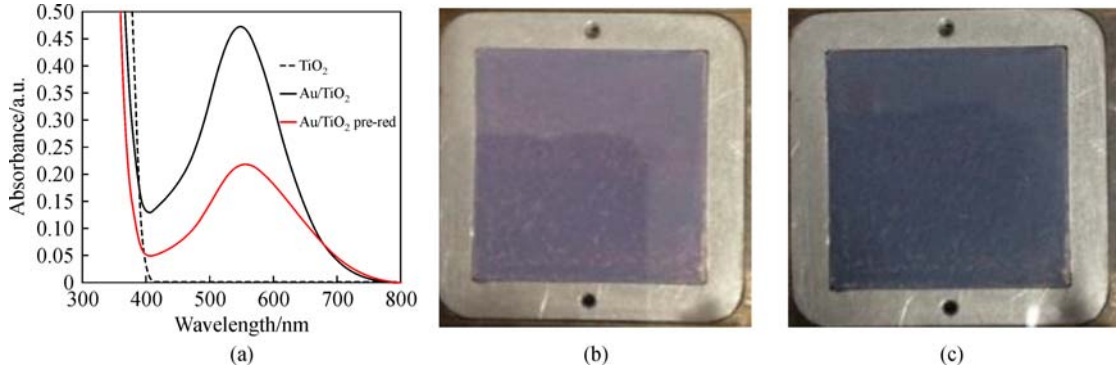

Fig. 2 LSPR absorption of around 550 nm for catalyst films

(a) Absorption spectra for Au/TiO_2 catalyst films; (b) the red line is the results before H_2 treatment; (c) black line is the result after H_2 treatment (Reprinted from Ref. [47] with permission from American Chemical Society.)

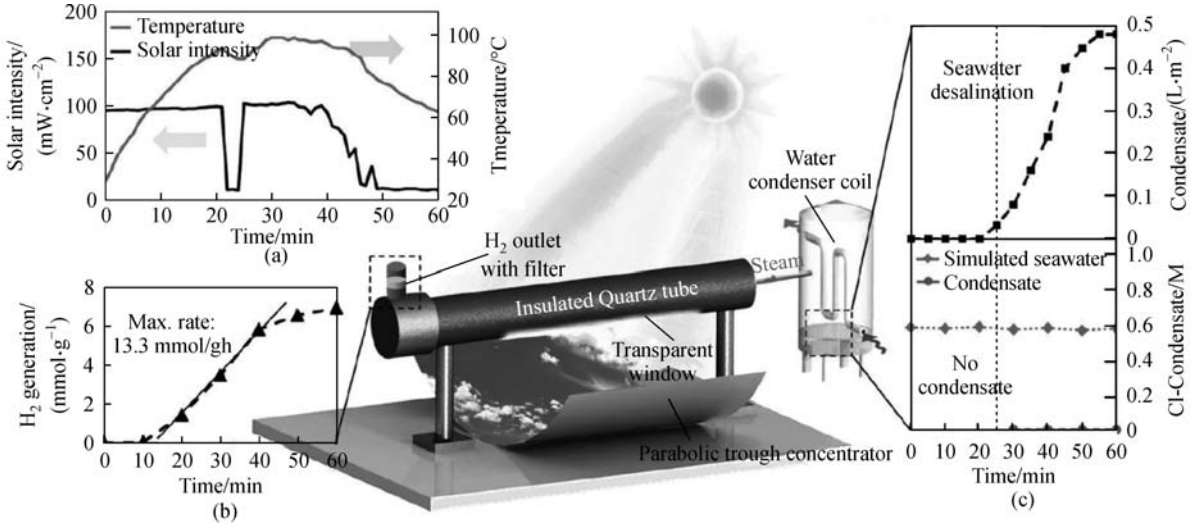

Fig. 3 Schematic of the prototype reactor with measurement of the time dependent graph
(a) Solar intensity and temperature; (b) hydrogen generation; (c) volume of the condensate (top) and chlorine concentration (bottom) (Reproduced from Ref. [48] under Creative Commons CC-BY license.)

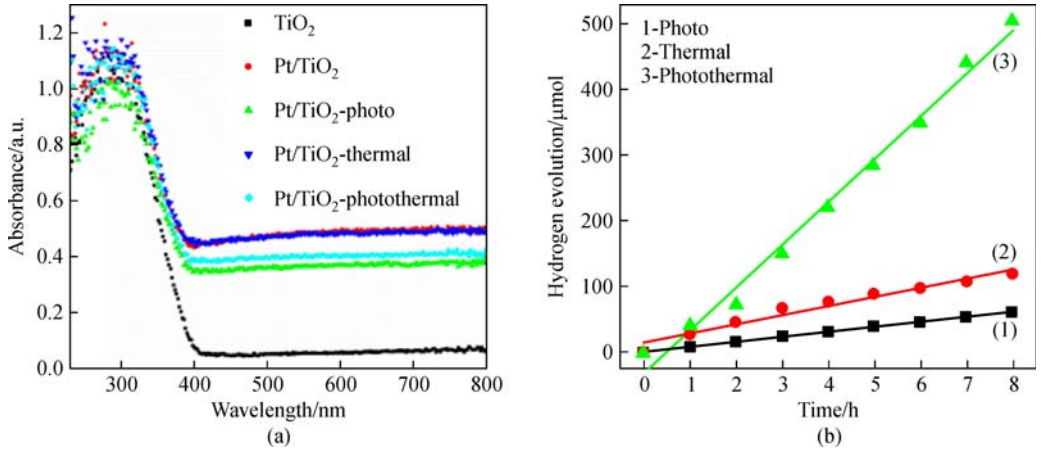

Fig. 4 Testing the properties of Pt/TiO_2 for photo-thermal synergy
(a) Absorbance of Pt/TiO_2 detected by UV-Vis diffuse reflectance spectra; (b) performances of photo-thermal catalysis, thermal catalysis and photo catalysis (Reproduced from Ref. [51] under Creative Commons CC-BY license.)

investigated the synergy of photo and thermal effects on Pt/TiO_2 catalyzed formic acid reforming [52].

For catalysts other than TiO_2, $Pt/SrTiO_3$ photocatalyst [53] was fabricated for hydrogen production from various alcohol or Na_2SO_3 solutions. A temperature range from 15°C to 45°C was applied, and the highest rate is 500 $\mu mol/(g_{cat}\cdot h)$ with a Pt loading of 0.5 wt% under UV light. Though Na_2SO_3 appeared to have the lowest activity (150 $\mu mol/(g_{cat}\cdot h)$), it is a cheap material from mines or seawater and has a great potential in application.

A recent research of photo-thermal synergetic reaction for hydrogen evolution was implemented with Pt/TiO_2 photocatalysts dispersed in aqueous solutions of ethylene glycol [36]. At a light intensity of 6500 W/m^2, the reaction temperature was controlled from 38°C to 60°C to test the sensibility of hydrogen production to heat. The results show that hydrogen production in 4 h peaked at 15.18 $mmol/g_{cat}$ at 55°C. Explanation of the peak was derived from thermodynamic deductions, although the optimal temperature remains complicated.

3.3 Alkanesor hydrogen as sacrificial reagents

3.3.1 Photocatalytic steam reforming of alkanes (PSRM)

Yoshida and coworkers showed that with UV lights (before 400 nm) and Pt/TiO_2, SRM is enabled to proceed around room temperature [54], instead of over 1073 K. They studied the effects of Pt loading, Pt size, light intensity, and CH_4 concentration. They continued loading Pt on other

eligible photocatalysts, such as $NaTaO_3$:M_{BM} [55], where M_{BM} was La, Gd, and Ybor Ba. The best observed photo-thermal activity was from Pt/$NaTaO_3$:La (2%), which was more than twice that of Pt/TiO_2.The thermal effects slightly increased the activity of Pt(0.03)/$NaTaO_3$:La_{BM} (2%) and plateaued after the temperature reached 350 K. Later in 2011, they found that the reaction rate over Pt/Ga_2O_3 [56] for PSRM was promoted by stepwise increasing temperature from 318 K to 344 K. The thermal activation energy was found to decrease with increasing light intensity. For example, the hydrogen yield at 318 K rose linearly as light intensity grew from 50 W/m^2 to 300 W/m^2.

3.3.2 CO_2 reforming of alkane (CRM)

CH_4 and CO_2 are both greenhouse gases inducing a growing environmental concern. CO_2 reforming of methane (CRM) can convert CH_4 and CO_2 mixture into solar fuels. In thermocatalysis, successive CRM requires a temperature of 800°C–1000°C to overcome the high reaction barrier associated. For solar fuels, this requires a large mirror field and durable reactors. Photo-thermal catalysis is expected to break the thermodynamic barrier of endothermic reaction, e.g. CRM, to occur at a lower temperature.

Photoreduction of CO_2 to CO by methane was reported to occur on ZrO_2 and MgO at room temperature [57,58]. However, H_2 was scarcely obtained from methane. Other products, such as H_2O and surface formate species, were acquired instead.

Yoshida's group did CRM over commercial Ga_2O_3 pretreated at 800°C in 13.3 kPa oxygen [59]. Such catalyst can operate CRM reactions at mild temperatures between 200°C and 400°C. The results show that the heating of catalyst may increase the activity under light irradiation. However, reactions did not occur in absence of light. It is speculated that the thermal effects would help the thermal steps with low activation energy in the photocatalytic CRM, e.g. desorption of products or migration of photo excited electron, while the main activation step on this CRM would be promoted by photo energy.

For LSPR enhancements on photo-thermal CRM, Au NPs were added to Rh/SBA-15 (made of SiO_2) catalysts [60]. All of the three catalysts have UV-Vis absorption in DRS spectra (Fig. 5(a)). The operation temperature was kept at 500°C by visible light irradiation in all reaction sets. The highest fuel yield over Au-Rh/SBA-15 is 6900 μmol/(g_{cat}·s) for H_2 and 6800 μmol/(g_{cat}·s) for CO_2, which is 1.7 times to that over Rh/SBA-15. As shown in Fig. 5(b) and (c), Au-Rh/SBA-15 has a fuel yield of nearly 1.5 times of the sum of yields from Rh/SBA-15 and Au/SBA-15 in the same condition, indicating the photo-thermal synergetic effect. However, with increasing light intensity, the H_2 yield peaked at 2800 W/m^2 and then began to decrease. This may result from the Au melting and aggregation induced by LSPR localized heat, since the Tammann temperature of Au NPs is as low as 395°C. Carbon deposition in CH_4 cleavage may deactivate catalyst with prolonged reaction time.

Black TiO_2 has a smaller bang gap than ordinary TiO_2 due to a generated donor level (Ti^{3+}). Such energy level meets the requirements of CRM over 150°C because of thermally-induced changes in CO_2/CH_4 redox potential. As an active co-catalyst, Pt was loaded on the black of TiO_2 to form photo-thermal catalysts [61]. In visible light from an AM 1.5G solar simulator at 1 sun, reaction started over Pt-black TiO_2 at 350°C, which was 200 K lower than thermocatalysis. The temperature dependence of quantum efficiency was studied at 550°C, 650°C, and 700°C and a peak of 64.9% was acquired at 650°C. This may result from a beneficial shift in redox potential at 650°C and a turnover to thermocatalysis above 650°C.

3.3.3 Methanation of CO or CO_2

Decomposition or reforming of alcohols or alkanes is useful in hydrogen generation. However, removal of CO or CO_2 from gaseous products consumes electricity. As an

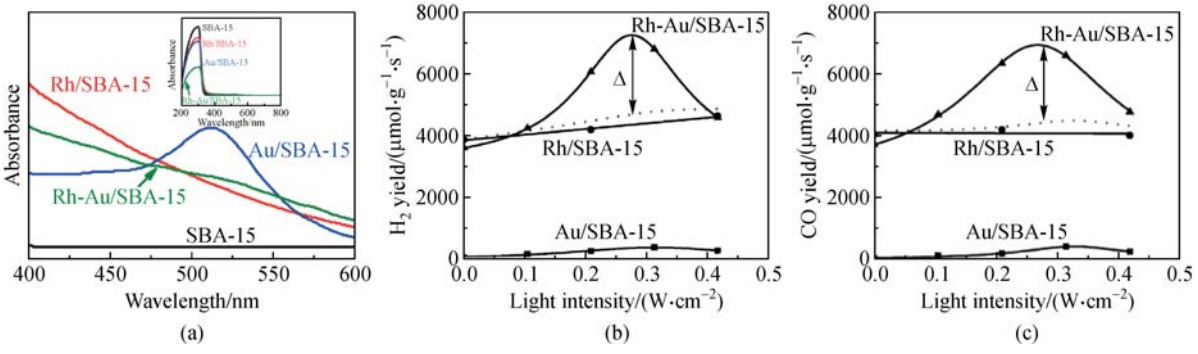

Fig. 5 Testing the properties of noble metal loaded SBA-15

(a) Absorption; (b) difference in activities of Rh/SBA-15, Au/SBA-15 and Au-Rh/SBA-15 shown in H_2; (c) CO yield. (Reproduced from Ref. [60] with permission from John Wiley and Sons.)

attractive strategy for the removal of CO in H_2-rich stream, Fu's group studied photothermal catalytic CO methanation over Ru/TiO_2 [62] and Ni/TiO_2 catalysts [63] in UV light from a Xenon lamp. They continued with CO_2 methanation over $Ru/TiO_{(2-x)}N_x$ catalysts assisted with visible light [22]. Figure 6(a) depicts the absorption spectra of $Ru/TiO_{(2-x)}N_x$ in comparisons with $TiO_{(2-x)}N_x$.

For reverse water-gas shift reactions(RWGS), Hoch and coworkers investigated UV-Vis responsive $In_2O_{3-x}(OH)_y$ calcinated at 250°C–450°C and operated at the optimal temperature of 150°C–190°C [64–65]. Then, they synthesized $In_2O_{3-x}(OH)_y$ NPs coated silicon nanowires (SiNWs) [66], realizing the dual function of utilizing both light and heat energy provided by the broad-band solar irradiance. To enhance the understanding of this reaction, the mechanism in photothermal hydrogenation of CO_2 gas was investigated on $Pd@Nb_2O_5$ nanocrystals [67].

Plasmonic Au NPs with an average diameter of 3.5 nm on various oxides were tested for their enhancement on activity [68]. Deposition of Au NPs expanded absorption of TiO_2, CeO_2, and Al_2O_3 to the visible light region, as shown respectively in Fig. 7(a)–(c). The temperature of the reaction was varied from 100°C to 400°C at constant pressure to test the CO_2 conversion rate. The results in Fig. 7(d) showed that light-induced LSPR enhanced thermal chemical performances, but the enhancements decreased with increasing temperature. The LSPR effect was suggested to change the energetics of the reaction because of an observed decrease in apparent activation energy (Fig. 7(e)). It was proposed that the changes were caused by either hot electron generation or adsorbate polarization.

Tahir et al. [69] analyzed nanostructured $NiO–In_2O_3/TiO_2$ catalyst for RWGS reaction. The effect of reaction temperatures of 100°C, 120°C, and 140°C was investigated to determine the effects of heating. They found that temperature rise gradually increased CH_4 production but decreased CO yield at elevated temperature (140°C).

Lights assistance in Sabatier reactions were studied over RuNPs supported on SiNW [70]. The as-synthesized catalyst absorbed Vis-NIR lights (Fig. 8(a)) and turned 4:1 mixture of H_2 and CO_2 to methane. Ina Xenon lamp light intensity of 3.2 sun and a temperature of 150°C, a maximum CO_2 conversion rate of 0.99 mmol/(g_{cat}·h) was achieved. After experiments at various wavelengths in Fig. 8(c), a photo-thermal synergetic mechanism was proposed. Sub-band gap photons generated heat and activated the thermal catalysis. Photos with an energy greater than band-gap induced electron-hole pairs in the SiNW support, then the pairs accelerated the reaction by activating adsorbed hydrogen atoms. The results also showed that thermal catalysis was in majority because the reaction rates were higher in lights with longer wavelengths (Fig. 8(d)).

3.4 Fuel production without sacrificial reagents

3.4.1 Direct water splitting

In 1995, the dependences of light intensity, Ph and temperature on water splitting were experimentally studied over $Pt\text{-}RuO_2/TiO_2$ to derive a kinetic model [8]. The intrinsic rate was found to be linearly dependent on the intensity of incident light P, exponentially dependent on the pH of reaction solution and on reciprocal temperature T. The mathematical expression is $r_i = K_p K_{\mathrm{pH}} K_T = k_p P \cdot k_{\mathrm{pH}} e^{\alpha \mathrm{pH}} \cdot k_T e^{-E/RT} = k_0 e^{\alpha \mathrm{pH}} e^{-E/RT} P$, where α, k_0, E are constants. The value of α is 0.19, while the value of activation energy E is 27 kJ/mol, 18.5 kJ/mol, and 21 kJ/mol for anatase, rutile and P25 TiO_2. The value of k_0 is derived from the experimental data.

Hisatomi et al. [71] examined the reaction activity of

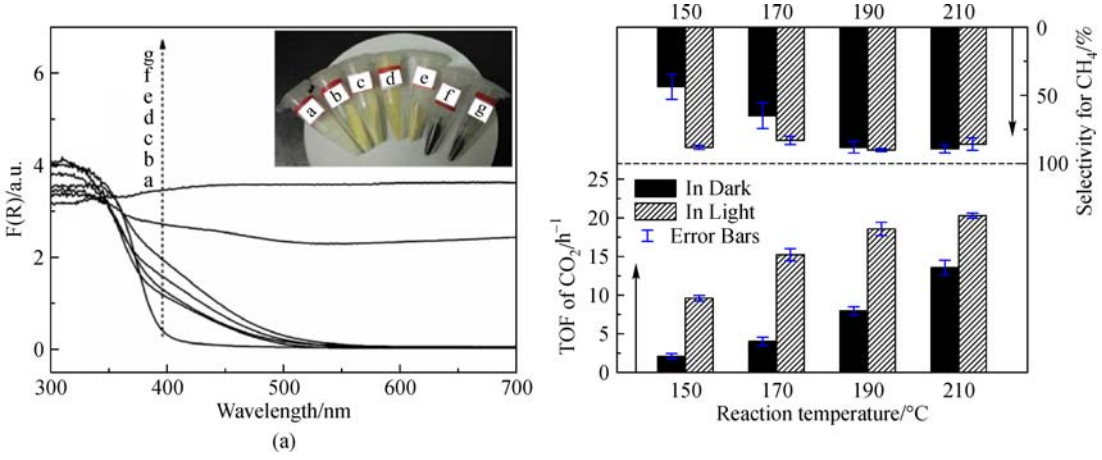

Fig. 6 Testing the properties of $Ru/TiO_{(2-x)}N_x$

(a) DRS spectra and appearance of $Ru/TiO_{(2-x)}N_x$, labeled f and g; (b) TOF (the turnover number of CO to CO_2 per Ru atom per second) of CO_2 and selectivity of CH_4 (Reprinted from Ref. [22] with permission from Elsevier.)

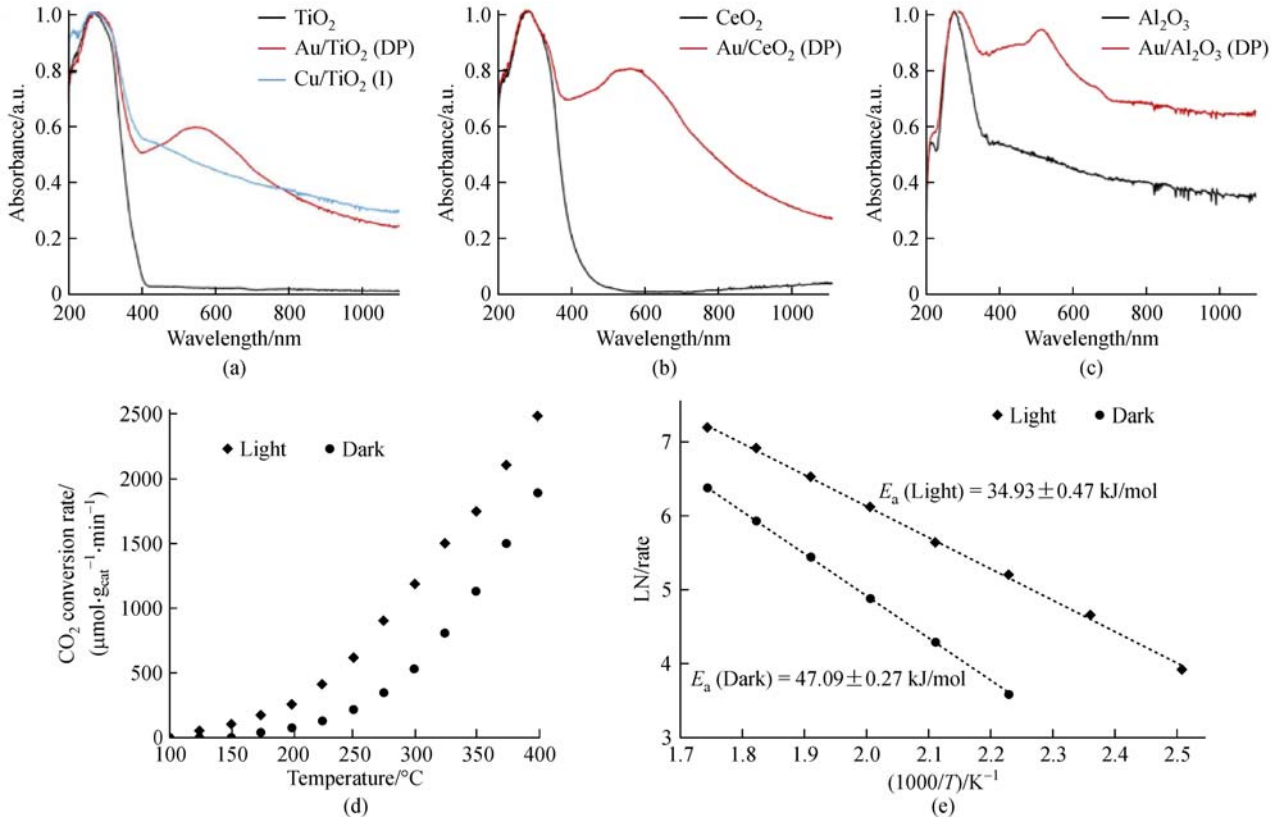

Fig. 7 Absorbance

(a) Au/TiO_2; (b) Au/CeO_2; (c) Au/Al_2O_3; (d) temperature dependence of reaction rate in light and dark conditions; (e) decrease of apparent activation energy caused by LSPR (Reproduced from Ref. [68] with permission from The Royal Society of Chemistry.)

water splitting over $Rh_{2-y}Cr_yO_3$ loaded $(Ga_{1-x}Zn_x)(N_{1-x}O_x)$ when the reaction was affected by variations in co-catalyst loading, light intensity, hydrogen/deuterium isotopes, and reaction temperature. They also studied the dependence of H_2 yield on temperature over $Rh_{2-y}Cr_yO_3$ loaded Ga_2O_3: Zn [72].The water splitting rates monotonically increased from 300 μmol/($h \cdot g_{cat}$) to 387 μmol/($g_{cat} \cdot h$) with increasing reaction temperature in the range from 5°C to 50°C.

The manganese/semiconductor catalyst is highly sensitive to temperature and irradiation shifts [73]. An elevated temperature between 25°C and 85°C can cause decomposition of the Mn(III/IV)-oxo dimer [74] and increase absorption, resulting in increased absorption in three regions of 280 nm, 310 nm–340 nm, and 400–440 nm. Nanostructures and mechanisms for manganese-containing compounds to mimic natural photosynthesis were summarized in details [75].

3.4.2 CO_2 reduction into fuels

Different from RWGS or chemical cycles, CO_2 reduction without consumption of sacrificial reagents was listed here. Hydrogen treated mesoporous WO_3 [76] was applied at relatively low temperatures (< 300°C) to convert CO_2 and water to CH_4 or CH_3OH invisible light (> 420 nm).The catalysts exhibit a selectivity toward CH_4 evolution in only visible light irradiation. Under photo-thermal conditions, the concentration of oxygen vacancies significantly influenced the performance. In chemical engineering, rational reactor design is beneficial for efficient CO_2 photo-thermal coupled reduction. A three-dimensional numerical optimization was applied on a solar parabolic trough receiver reactor (SPTRR) filled with catalysts [77]. The results showed that a more uniform distribution of outer surface temperature and a higher chemical energy conversion per unit pump power were acquired. A modified concentrated solar reactor was developed to test the performance of CO_2 reduction experimentally [78].

For solar photo-thermochemical alkane reverse combustion (SPARC) processes to produce C1 to C13 hydrocarbons, a one-step, gas-phase reaction with $Co(5\%)/TiO_2$ catalysts [79] was conducted at 180°C–200°C under UV irradiation. A parametric study of pressure and partial pressure ratio revealed that temperatures in excess of 160°C were needed to obtain a higher Cn products in quantity and that the product distribution shifted toward higher Cn products with increasing pressure. However,

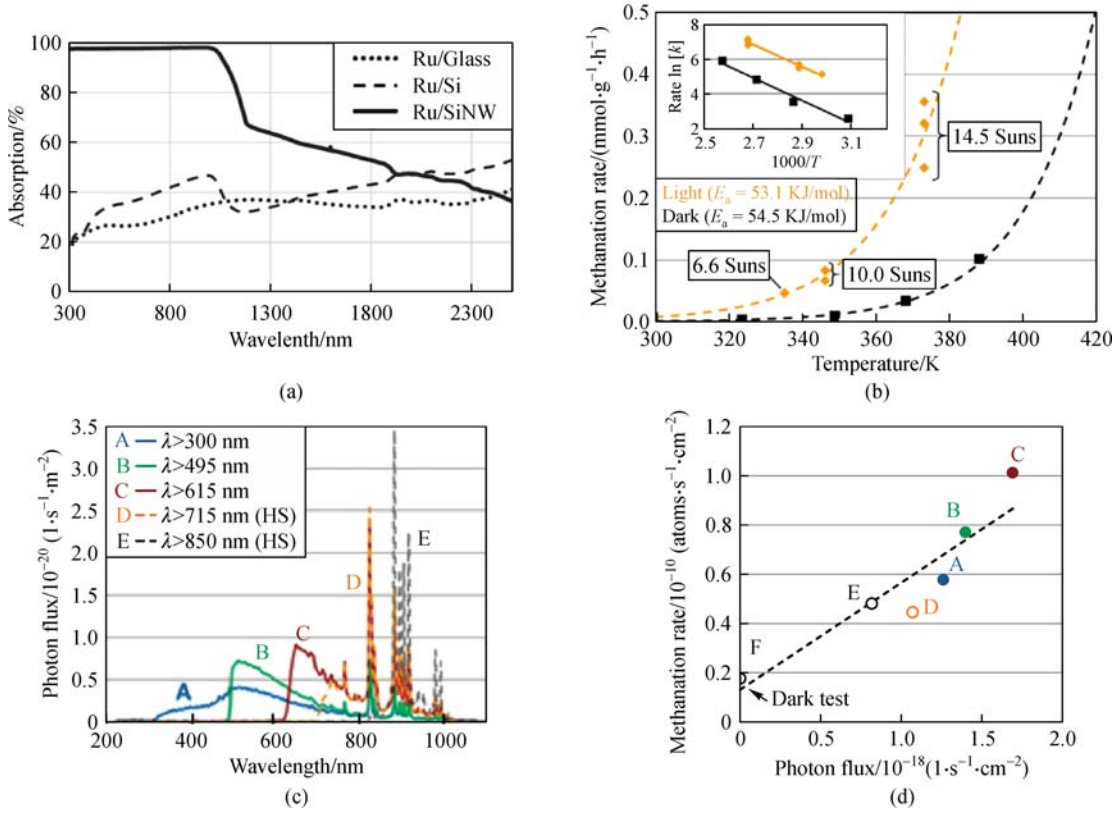

Fig. 8 Test of photocatalytic activity in different conditions

(a) Absorption spectra for Ru deposited Si, glass and SiNW supports; (b) methanation rates ln$k$ plotted as a function of temperature T in the dark (black) and under solar-simulated irradiation (yellow) (The inset shows these methanation rates on a plot of ln$k$ versus 1000 T^{-1} used to calculate the activation energy); (c) spectra of different lights used in experiments; (d) corresponding results (Reprinted from Ref. [71] with permission from John Wiley and Sons.)

solar-to-fuel efficiency of this process was not commercially applicable and needed to be increased.

3.4.3 Light-assisted high temperature solar fuel production cycles

T-Raissi et al. [80] analyzed light assisted high temperature CO_2/CO cycle and SO_2/sulfuric acid cycles. The CO_2/CO cycle is based on the premise that CO_2 becomes susceptible to near-UV and even visible radiation at high temperatures (greater than 1300 K). Depicted in Fig. 9(a), SO_2/sulfuric is a modification of Westinghouse hybrid cycle, wherein the electrochemical step is replaced by a photocatalytic step. The results showed that SO_2/sulfuric required no electricity input and a maximum temperature lower than 1170 K, compared to the traditional Westinghouse hybrid cycle. A solar energy system was constructed based on the SO_2/sulfuric acid cycle (see Fig. 9(b)).

Thermally-driving chemical-looping is widely studied such as ZnO/Zn,SnO_2/SnO, and Fe_3O_4/FeO cycles for solar fuels. However, two-step water-splitting chemical-looping was also enhanced by light irradiation. Under 1 sun, a Cu-loaded TiO_2 enabled the oxygen expulsion at room temperature and H_2 release from steam to take place at 140°C [81]. Absorption of TiO_2 was extended to 450 nm, but visible and infrared light were also utilized due to photo-thermal effects. Optimized loading of Cu was 1%, and H_2 and O_2 yields decrease by 11%–13% after 25 cycles. In a 6 cm^2 reactor containing 0.25 g catalysts, the hydrogen yield of 4 μmol/(cm^2·h) was acquired. The conversion efficiency was 0.25 at 1 sun and had the potential to be further optimized.

A CO_2 reduction cycle was experimentally studied and modeled using the density functional theory to probe the efficacy of MnO_x nanoclusters surface modification of rutile and anatase [82]. The MnO cycled between Mn^{3+} and $Mn^{2+}$with inputs of thermal and photo energy using CO_2 to produce CO and heal oxygen vacancies.

3.5 Forms of photocatalysts

Photo-thermal catalysts are usually in the scale of millimeter or nanometer to acquire a high specific surface area. When applied in liquid phase reactions, catalyst NPs

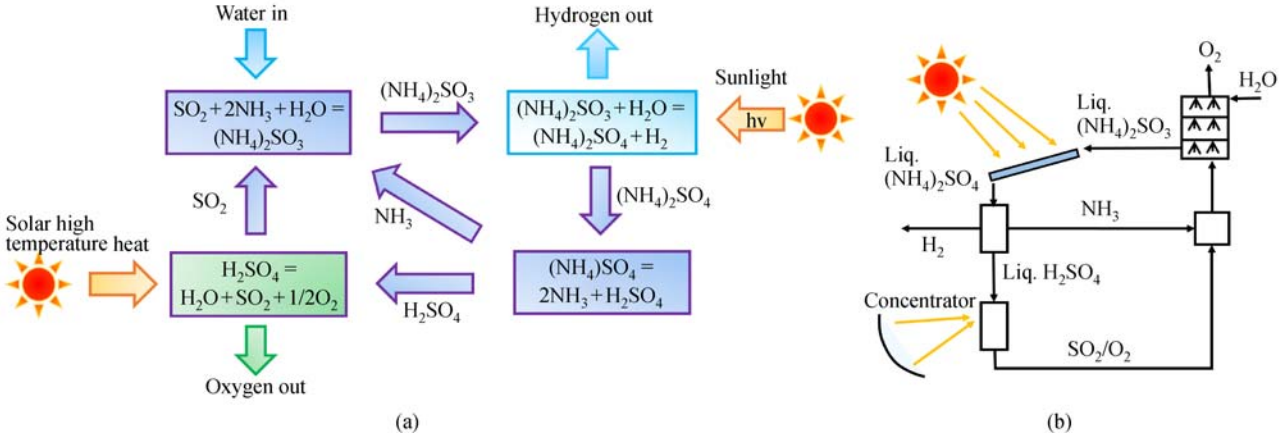

Fig. 9 Hydrogen production from sunlight through the SO_2/sulfuric acid cycle
(a) Diagram of the SO_2/sulfuric acid cycle; (b) system design for sunlight to hydrogen conversion

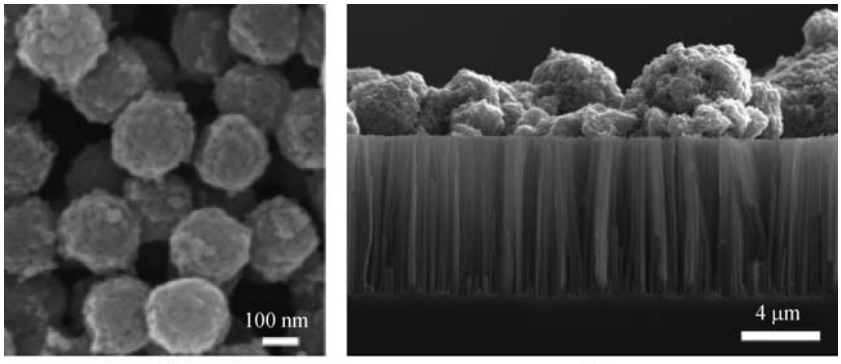

Fig. 10 SEM images
(a) Si/Ag@TiO_2 NPs [48]; (b) $In_2O_{3-x}(OH)_y$ NPs coated SiNWs (Reproduced from Refs. [48] and [66] under Creative Commons CC-BY license)

(see Fig. 10(a)) are dispersed to form a stable mixture, providing a high contact area between the catalyst and reactants. A stable liquid mixture also works as a homogeneous selective filter of induced light, which is important to eliminate "hot spots" in underlying PV arrays or thermal receivers.

In circumstances of elevated temperatures or gas phase reactions, dramatic movements and relatively high surface energy of particles may cause agglomeration of catalysts and reduce reaction activity as well as light selectivity. To ensure stability, catalysts are deposited upon substrates like SiO_2 chips, films, or nanowires, like Fig. 10(b). Requirements for substrates are made on light absorption, specific surface area, and thermal endurance. Morphologies of deposited catalysts like arrays of nanosheets, nanotubes, and nanorods are developed for efficient light trapping. However, light absorption here is on the surface of deposited catalysts rather than volumetric in liquids, thus a rational design of reaction bed and reactor is still required.

4 Summary

The works reviewed from Sub-section 3.1 to 3.3 are listed in Table 1. The works reviewed in Sub-section 3.4 are listed in Table 2.The representative data highlighted by the authors are presented. The short dash stands for the data that are not given in literature.

5 Potential and challenges

The photo-thermal catalytic reactions with spectrum-selectivity are emerging methods of solar fuel production. Photo-thermal catalysis is the synergetic effect rather than the superposition of photo and thermal catalyzes. Performances of photo-thermal catalysis are usually reported to be higher than photo or thermal catalysis, while the underlying mechanism remains unclear and needs further exploration. Due to its spectrum selective nature, the photo-thermal catalysis reaction is more applicable in full-

Table 1 Summary of photo-thermal catalytic reactions with spectrum-selectivity and sacrificial reagents

Reference	Catalyst	Preparation methods	Light absorption	Light Source and intensity	Temperature (°C) /Pressure (atm)	Reactants/Reactions	Yields
Liu et al. [10]	1 wt.% Pt/TiO_2	Photo-deposited	–	300 W Xenon lamp UV-Vis-IR	54/–	50 mL of 10 vol.% methanol aqueous solution	H_2, 22 mmol/(g_{cat}·h)
Mangrulkar et al. [11]	Nanocomposite of Zn/ZnO and 10 mg carbonic anhydrase	Directly mixed	Before 400 nm and a peak around 800 nm	two 200 W tungsten filament lamps	70–80/–	100 mL of CO_2 saturated water	H_2, 1.238 mmol/(g_{cat}·h)
Nikitenko et al. [17]	$Ti@TiO_2$	Primary passivation of Ti nanopowder and crystallization of TiO_2 nanoparticles at the surface of metallic Ti core.	> 80% from UV to NIR region	100 W halogen lamp 500 $W \cdot m^{-2}$	60/–	10 mL of 25 vol. % methanol aqueous solution	H_2, 0.468 mmol/(g_{cat}·h)
Liang et al. [36]	Pt/TiO_2	Photo-deposited	Before 400 nm	300 W Xenon lamp 6500 $W \cdot m^{-2}$	55/–	100 mL aqueous solutions containing 0.02 mL ethylene glycol	H_2, 3.795 mmol/(g_{cat}·h)
Gao et al. [48]	$SiO_2/Ag@TiO_2$	SiO_2/Ag: Stöber method TiO_2 coating: sol-gel method	Full spectrum	Real sun, 1 sun	100/1	300 mL of 20 vol.% glycerol with 10.5 g of sodium chloride	H_2, 13.3 mmol/(g_{cat}·h)
Song et al. [51]	Non plasmonic Pt/TiO_2	*In situ* photodecomposition	> 70% (< 400 nm) = 70% (400–800 nm)	Purple LED light	90/–	120 mL of 10 vol.% HCOOH aqueous solution	H_2, 714.3 μmol/(g_{cat}·h)
Puangpetch et al. [53]	0.5 wt.% Pt-loaded $SrTiO_3$	Mesoporous-assembled	Before 450 nm	176 W Hg lamps	45/–	500 mL of 50 vol.% methanol aqueous solution	H_2, 500 μmol/(g_{cat}·h)
						500 mL of 1 mol/L Na_2SO_3 aqueous solution	H_2, 170 μmol/(g_{cat}·h)
Shimura et al. [55]	$Pt(0.1)/NaTaO_3$:La(2%)	Solid-state reaction method; impreganation method for Pt loading	Before 320 nm	300W Xenon lamp	140/1	10% CH_4, 1% H_2O with Ar carrier gas with total flow rate of 50 mL/min	H_2, 270 μmol/(g_{cat}·h)
Shimura et al. [56]	$Pt(7\%)/Ga_2O_3$	Homogeneous precipitation for Ga_2O_3, impreganation method for Pt loading	–	300 W Xenon lamp	71/–	Mixture of water vapor and methane with total flow rate of 40 mL/min	H_2, 50.3 μmol/(g_{cat}·h) CO, 3.82 μmol/(g_{cat}·h) and hydrocarbon < 1 μmol/(g_{cat}·h)
Yuliati et al. [59]	β-Ga_2O_3	Commercial products pretreated at 1073 K in 13.3 kPa oxygen	–	300 W Xenon lamp	400/–	400 μmol of 1:1 (molar ratio) CH_4 and CO_2	H_2, 10.53 μmol/(g_{cat}·h)
Liu et al. [60]	Rh-Au/SBA-15	Au deposition: precipitation method; Rude position: impregnation method	Before 600 nm	300 W Xenon lamp, 3000 W/m^2	500/–	1:1 CH_4:CO_2 with total flow rate of 20 mL/min	H_2: 414 mmol/(g_{cat}·h) CO: 408 mmol/(g_{cat}·s)

(*Continued*)

Reference	Catalyst	Preparation methods	Light absorption	Light Source and intensity	Temperature (°C) /Pressure (atm)	Reactants/Reactions	Yields
Han et al. [61]	Black TiO_2 on light diffuse-reflection surface	Hydrogenation	Peak before 400 nm, relatively strong before 800 nm	AM 1.5G, 1000 W/m^2, UV light filtered	650/–	1:1 CH_4: CO_2 with total flow rate of 10 mL/min	H_2, 129 mmol/(g_{cat}·h) CO, 370 mmol/(g_{cat}·h)
Ghuman et al. [65]	Hydroxylated $In_2O_{3-x}(OH)_y$	Temperature controlled decomposition of $In(OH)_3$	> 90%(< 400 nm) = 20% (400–800 nm)	300W Xe lamp 2200 W/m^2	150/3	1:1 CO_2: H_2 with total flow rate of 6 mL/min	CO,15 μmol/(g_{cat}·h)
Hoch et al. [66]	Evenly coated $In_2O_{3-x}(OH)_y$ /SiNW film	Metal assisted chemical etching for nanowires	> 95% (full spectrum)	300 W Xe lamp ~20 kW/m^2	150/2	12 mL of 1:1 CO_2 and H_2	CO, 22 μmol/(g_{cat}·h)
Jia et al. [67]	Ru/SiNW	Metalassistedchemical etching for nanowires	> 70% before 1100 nm, > 40% before 2500 nm	Xe lamp 25 kW/m^2	160/1.84	1.8 mL of 4:1 H_2 and CO_2	CO, 4.9 mmol/(g_{cat}·h)
Lin et al. [62]	Ru/TiO_2	Facile impregnation reduction method.	Before 600 nm	UV light irradiation from a Xenon lamp	200/1	0.5 vol.% CO, 20.0 vol. % H_2 and balance He, with total flow rate of 100 mL/min	(CO conversion 100%)
Lin et al. [63]	Ni/TiO_2	Facile impregnation reduction method	Before 400 nm		250/1	1 vol.% CO, 39 vol.% H_2, and balance gas He with total flow rate of 100 mL/min	(CO conversion 100%)
Lin et al. [22]	Ru/$TiO_{(2-x)}N_x$	Sol-gel method	Full spectrum	Visible light	190/1	0.6 vol. % CO_2, 2.4 vol.% H_2, and t balance gas He with total flow rate of 60 mL/min	20 (turned CO over per Ru atom per hour)
Upadhye et al. [68]	Au-TiO_2(DP)	Deposition-precipitation method	> 65% before 700 nm	Visible light 5216 W/m^2	400/7.49	2:1 H_2 and CO_2 with total flow rate of 15 mL/min	CO_2 reduction 2.663 mmol/(g_{cat}·h)

Table 2 Summary of photo-thermal catalytic reactions with spectrum-selectivity but without sacrificial reagents

Reference	Photothermal catalysts	Light absorption	Light source and intensity	Temperature (°C)/ Pressure(atm)	Reactants or reactions	Yields
Hisatomi et al. [72]	$Rh_{2-y}Cr_yO_3$ loaded Ga_2O_3:Zn	–	300 W Xe lamp (200–500 nm)	72/–	140 mL of distilled water	H_2, 387 μmol/(g_{cat}·h); O_2, ~194 μmol/(g_{cat}·h)
Wang et al. [76]	m-WO_3 treated in H_2 at 250°C	UV-Vis light	300 W Xenon lamp (> 420 nm)	250/–	120 mL of H_2O and CO_2 mixture	CH_4 2.083 μmol/(g_{cat}·h), CH_3OH 0.208 μmol/(g_{cat}·h)
Wang et al. [76]	m-WO_3 treated in H_2 at 550°C	UV-Vis light	300 W Xenon lamp (> 420 nm)	250/–	120 mL of H_2O and CO_2 mixture	CH_4 0.417 μmol/(g_{cat}·h), CH_3OH 0.83 μmol/(g_{cat}·h)
Chanmanee et al. [79]	5%Co/TiO_2	–	4 surrounding 250 W Hg lamps	200/6.1	p(H_2O)/p(CO_2) = 0.6, with total flow rate of 40 mL/min	O_2 40 μg/(g_{cat}·h), hydrocarbon 10 μg/(g_{cat}·h), H_2 2 μg/(g_{cat}·h)
Docao et al. [81]	Cu(1.0)/TiO_2	Before 420 nm	AM 1.5 G solar simulator, 3 suns	Room temperature for water splitting, 140 for reduction of oxide	Water steam with N_2 carrier gas	4 μmol/(cm^2·h) (0.25 g catalyst, irradiated area = 6 cm^2)

spectrum solar energy systems when coupled with PV arrays or power cycles. According to Section 3, such reactions produce solar fuels from a wide variety of reactants, such as biomass, fossil fuels, sewages, water and CO_2, which suggests the feasibility satisfying the industrial requirements in nowadays and the future.

As a newly-proposed type of reaction, spectrum-selective photo-thermal catalytic reaction yet demands for more academic attentions. Research directions may be as follows:

1) Optimizations on materials and structure of catalysts are needed to achieve a higher conversion efficiency and selectivity of products.

2) Consider the integration with other energy conversions, simple and cheap ways to alter catalyst light absorption should be developed.

3) Deeper understanding of the reaction mechanism, especially the photo-thermal synergy effects, is expected to be explored.

4) Elevated temperature is likely to induce deactivation of catalysts. Therefore, high-temperature durability is expected.

Acknowledgements This work was supported by the National Natural Science Foundation of China (Grant Nos. 51406205 and 51236008).

References

1. Harvey P R, Rudham R, Ward S. Photocatalytic oxidation of liquid 2-propanol by titanium dioxide. Journal of the Chemical Society, Faraday Transactions 1: Physical Chemistry in Condensed Phases, 1983, 79(6): 1381–1390
2. Okamoto K, Yamamoto Y, Tanaka H, Itaya A. Kinetics of heterogeneous photocatalytic decomposition of phenol over anatase TiO_2 powder. Bulletin of the Chemical Society of Japan, 1985, 58 (7): 2023–2028
3. Chen L C, Chou T C. Kinetics of photodecolorization of methyl-orange using titanium-dioxide as catalyst. Industrial & Engineering Chemistry Research, 1993, 32(7): 1520–1527
4. Vorontsov A V, Stoyanova I V, Kozlov D V, Simagina V I, Savinov E N. Kinetics of the photocatalytic oxidation of gaseous acetone over platinized titanium dioxide. Journal of Catalysis, 2000, 189(2): 360–369
5. Yamazoe S, Hitomi Y, Shishido T, Tanaka T. Kinetic study of photo-oxidation of NH_3 over TiO_2. Applied Catalysis B: Environmental, 2008, 82(1–2): 67–76
6. Hussein F H, Rudham R. Photocatalytic dehydrogenation of liquid alcohols by platinized anatase. Journal of the Chemical Society, Faraday Transactions I, 1987, 83(5): 1631–1639
7. Naito S. Study of photocatalytic reaction of methanol with water over Rh-loaded, and Pd-loaded TiO_2 catalysts—the role of added alkali-metal cations. Canadian Journal of Chemistry-Revue Canadienne De Chimie, 1986, 64(9): 1795–1799
8. Karakitsou K, Verykios X E. Definition of the intrinsic rate of photocatalytic cleavage of water over Pt-RuO_2/TiO_2 catalysts. Journal of Catalysis, 1995, 152(2): 360–367
9. Zhang J, Tang Y L, Hu G, Gao B L, Gan Z X, Chu P K. Carbon nanodots-based nanocomposites with enhanced photocatalytic performance and photothermal effects. Applied Physics Letters, 2017, 111(1): 013904
10. Liu X, Ye L, Ma Z, Han C, Wang L, Jia Z, Su F, Xie H. Photothermal effect of infrared light to enhance solar catalytic hydrogen generation. Catalysis Communications, 2017, 102: 13–16
11. Mangrulkar P A, Chilkalwar A A, Kotkondawar A V, Manwar N R, Antony P S, Hippargi G, Labhsetwar N, Trachtenberg M C, Rayalu S S. Plasmonic nanostructured Zn/ZnO composite enhances carbonic anhydrase driven photocatalytic hydrogen generation. Journal of CO2 Utilization, 2017, 17: 207–212
12. Panayotov D A, Morris J R. Surface chemistry of Au/TiO_2: thermally and photolytically activated reactions. Surface Science Reports, 2016, 71(1): 77–271
13. Wentworth W E, Batten C F, Wei G. The photo-assisted thermal decomposition of methanol and isopropanol in a fluidized bed. Energy, 1987, 12(3–4): 319–331
14. Yu S, Zhang T, Xie Y, Wang Q, Gao X, Zhang R, Zhang Y, Su H. Synthesis and characterization of iron-based catalyst on mesoporous titania for photo-thermal F-T synthesis. International Journal of Hydrogen Energy, 2015, 40(1): 870–877
15. Verma R, Samdarshi S K, Bojja S, Paul S, Choudhury B. A novel thermophotocatalyst of mixed-phase cerium oxide (CeO_2/Ce_2O_3) homocomposite nanostructure: role of interface and oxygen vacancies. Solar Energy Materials and Solar Cells, 2015, 141: 414–422
16. Huang K, Lin L, Yang K, Dai W, Chen X, Fu X. Promotion effect of ultraviolet light on NO + CO reaction over Pt/TiO_2 and Pt/CeO_2-TiO_2 catalysts. Applied Catalysis B: Environmental, 2015, 179: 395–406
17. Nikitenko S I, Chave T, Cau C, Brau H P, Flaud V. Photothermal hydrogen production using noble-metal-free Ti@TiO_2 core–shell nanoparticles under Visible–NIR light irradiation. ACS Catalysis, 2015, 5(8): 4790–4795
18. Ren J, Ouyang S, Xu H, Meng X, Wang T, Wang D, Ye J. Targeting activation of CO_2 and H_2 over Ru-loaded ultrathin layered double hydroxides to achieve efficient photothermal CO_2 methanation in flow-type system. Advanced Energy Materials, 2017, 7(5): 1601657
19. Kho E T, Tan T H, Lovell E, Wong R J, Scott J, Amal R. A review on photo-thermal catalytic conversion of carbon dioxide. Green Energy & Environment, 2017, 2(3): 204–217
20. Delasa H, Rosales B S. Photocatalytic Technologies. Beijing: Science Press, 2010
21. Li Y, Wang C, Zheng H, Wan F, Yu F, Zhang X, Liu Y. Surface oxygen vacancies on WO_3 contributed to enhanced photothermo-synergistic effect. Applied Surface Science, 2017, 391, Part B: 654–661
22. Lin L, Wang K, Yang K, Chen X, Fu X, Dai W. The visible-light-assisted thermocatalytic methanation of CO_2 over Ru/$TiO_{(2-x)}N_x$. Applied Catalysis B: Environmental, 2017, 204: 440–455
23. Xie S, Wang Z, Cheng F, Zhang P, Mai W, Tong Y. Ceria and ceria-based nanostructured materials for photoenergy applications. Nano Energy, 2017, 34: 313–337

24. Kale M J, Avanesian T, Christopher P. Direct photocatalysis by plasmonic nanostructures. ACS Catalysis, 2014, 4(1): 116–128
25. Wang C, Ranasingha O, Natesakhawat S, Ohodnicki P R, Andio M, Lewis J P, Matranga C. Visible light plasmonic heating of Au-ZnO for the catalytic reduction of CO_2. Nanoscale, 2013, 5(15): 6968–6974
26. Looser R, Vivar M, Everett V. Spectral characterisation and long-term performance analysis of various commercial heat transfer fluids (HTF) as direct-absorption filters for CPV-T beam-splitting applications. Applied Energy, 2014, 113: 1496–1511
27. Draine B T, Flatau P J. Discrete-dipole approximation for scattering calculations. Journal of the Optical Society of America. A, Optics, Image Science, and Vision, 1994, 11(4): 1491–1499
28. Oubre C, Nordlander P. Optical properties of metallodielectric nanostructures calculated using the finite difference time domain method. Journal of Physical Chemistry B, 2004, 108(46): 17740–17747
29. Bohren C F, Huffman D R. Absorption and Scattering of Light by Small Particles. New York: Wiley, 1986
30. Duan H, Xuan Y. Enhanced optical absorption of the plasmonic nanoshell suspension based on the solar photocatalytic hydrogen production system. Applied Energy, 2014, 114: 22–29
31. Tauc J, Grigorovici R, Vancu A. Optical properties and electronic structure of amorphous germanium. Physica Status Solidi, 1966, 15 (2): 627–637 (b)
32. Ren L, Mao M, Li Y, Lan L, Zhang Z, Zhao X. Novel photothermocatalytic synergetic effect leads to high catalytic activity and excellent durability of anatase TiO_2 nanosheets with dominant {001} facets for benzene abatement. Applied Catalysis B: Environmental, 2016, 198: 303–310
33. Ohtani B. Revisiting the fundamental physical chemistry in heterogeneous photocatalysis: its thermodynamics and kinetics. Physical Chemistry Chemical Physics, 2014, 16(5): 1788–1797
34. Archer M D, Bolton J R. Requirements for ideal performance of photochemical and photovoltaic solar energy converters. Journal of Physical Chemistry, 1990, 94(21): 8028–8036
35. Liu B, Zhao X. A kinetic model for evaluating the dependence of the quantum yield of nano-TiO_2 based photocatalysis on light intensity, grain size, carrier lifetime, and minority carrier diffusion coefficient: indirect interfacial charge transfer. Electrochimica Acta, 2010, 55 (12): 4062–4070
36. Liang H, Wang F, Cheng Z, Hu S, Xiao B, Gong X, Lin B, Tan J, Li X, Cao R, Liang W, Liu L. Analyzing the effects of reaction temperature on photo-thermo chemical synergetic catalytic water splitting under full-spectrum solar irradiation: an experimental and thermodynamic investigation. International Journal of Hydrogen Energy, 2017, 42(17): 12133–12142
37. Fuentes M, Vivar M, Scott J, Srithar K, Skryabin I. Results from a first autonomous optically adapted photocatalytic-photovoltaic module for water purification. Solar Energy Materials and Solar Cells, 2012, 100: 216–225
38. Vivar M, Fuentes M, Dodd N, Scott J, Skryabin I, Srithar K. First lab-scale experimental results from a hybrid solar water purification and photovoltaic system. Solar Energy Materials and Solar Cells, 2012, 98: 260–266
39. Vivar M, Skryabin I, Everett V, Blakers A. A concept for a hybrid solar water purification and photovoltaic system. Solar Energy Materials and Solar Cells, 2010, 94(10): 1772–1782
40. Zamfirescu C, Dincer I. Assessment of a new integrated solar energy system for hydrogen production. Solar Energy, 2014, 107: 700–713
41. Coridan R H, Nielander A C, Francis S A, McDowell M T, Dix V, Chatman S M, Lewis N S. Methods for comparing the performance of energy-conversion systems for use in solar fuels and solar electricity generation. Energy & Environmental Science, 2015, 8 (10): 2886–2901
42. Christopher K, Dimitrios R. A review on exergy comparison of hydrogen production methods from renewable energy sources. Energy & Environmental Science, 2012, 5(5): 6640–6651
43. Ni M, Leung M K H, Leung D Y C, Sumathy K. A review and recent developments in photocatalytic water-splitting using TiO_2 for hydrogen production. Renewable & Sustainable Energy Reviews, 2007, 11(3): 401–425
44. Adleman J R, Boyd D A, Goodwin D G, Psaltis D. Heterogenous catalysis mediated by plasmon heating. Nano Letters, 2009, 9(12): 4417–4423
45. Christopher P, Xin H, Linic S. Visible-light-enhanced catalytic oxidation reactions on plasmonic silver nanostructures. Nature Chemistry, 2011, 3(6): 467–472
46. Marimuthu A, Zhang J, Linic S. Tuning selectivity in propylene epoxidation by plasmon mediated photo-switching of Cu oxidation state. Science, 2013, 339(6127): 1590–1593
47. Tan T H, Scott J, Ng Y H, Taylor R A, Aguey-Zinsou K F, Amal R. Understanding plasmon and band gap photoexcitation effects on the thermal-catalytic oxidation of ethanol by TiO_2-supported gold. ACS Catalysis, 2016, 6(3): 1870–1879
48. Gao M, Connor P K N, Ho G W. Plasmonic photothermic directed broadband sunlight harnessing for seawater catalysis and desalination. Energy & Environmental Science, 2016, 9(10): 3151–3160
49. He Y L, Xiao J, Cheng Z D, Tao Y B A. MCRT and FVM coupled simulation method for energy conversion process in parabolic trough solar collector. Renewable Energy, 2011, 36(3): 976–985
50. Cheng Z D, He Y L, Cui F Q, Xu R J, Tao Y B. Numerical simulation of a parabolic trough solar collector with nonuniform solar flux conditions by coupling FVM and MCRT method. Solar Energy, 2012, 86(6): 1770–1784
51. Song R, Luo B, Jing D. Efficient photothermal catalytic hydrogen production over nonplasmonic Pt metal supported on TiO_2. In: Proceeding of SPIE 9935, Solar Hydrogen and Nanotechnology XI, 2016, 9935,9935C
52. Song R, Luo B, Liu M, Geng J, Jing D, Liu H. Synergetic coupling of photo and thermal energy for efficient hydrogen production by formic acid reforming. AIChE Journal, 2017, 63(7): 2916–2925
53. Puangpetch T, Sreethawong T, Yoshikawa S, Chavadej S. Hydrogen production from photocatalytic water splitting over mesoporous-assembled $SrTiO_3$ nanocrystal-based photocatalysts. Journal of Molecular Catalysis A Chemical, 2009, 312(1–2): 97–106
54. Yoshida H, Hirao K, Nishimoto J I, Shimura K, Kato S, Itoh H, Hattori T. Hydrogen production from methane and water on platinum loaded titanium oxide photocatalysts. Journal of Physical Chemistry C, 2008, 112(14): 5542–5551
55. Shimura K, Kato S, Yoshida T, Itoh H, Hattori T, Yoshida H. Photocatalytic steam reforming of methane over sodium tantalate.

Journal of Physical Chemistry C, 2010, 114(8): 3493–3503
56. Shimura K, Maeda K, Yoshida H. Thermal acceleration of electron migration in gallium oxide photocatalysts. Journal of Physical Chemistry C, 2011, 115(18): 9041–9047
57. Kohno Y, Tanaka T, Funabiki T, Yoshida S. Reaction mechanism in the photoreduction of CO_2 with CH_4 over ZrO_2. Physical Chemistry Chemical Physics, 2000, 2(22): 5302–5307
58. Teramura K, Tanaka T, Ishikawa H, Kohno Y, Funabiki T. Photocatalytic reduction of CO_2 to CO in the presence of H_2 or CH_4 as a reductant over MgO. Journal of Physical Chemistry B, 2004, 108(1): 346–354
59. Yuliati L, Itoh H, Yoshida H. Photocatalytic conversion of methane and carbon dioxide over gallium oxide. Chemical Physics Letters, 2008, 452(1–3): 178–182
60. Liu H, Meng X, Dao T D, Zhang H, Li P, Chang K, Wang T, Li M, Nagao T, Ye J. Conversion of carbon dioxide by methane reforming under visible-light irradiation: surface-plasmon-mediated nonpolar molecule activation. Angewandte Chemie International Edition, 2015, 54(39): 11545–11549
61. Han B, Wei W, Chang L, Cheng P, Hu Y H. Efficient visible light photocatalytic CO_2 reforming of CH_4. ACS Catalysis, 2016, 6(2): 494–497
62. Lin X, Yang K, Si R, Chen X, Dai W, Fu X. Photo-assisted catalytic methanation of CO in H_2-rich stream over Ru/TiO_2. Applied Catalysis B: Environmental, 2014, 147: 585–591
63. Lin X, Lin L, Huang K, Chen X, Dai W, Fu X. CO methanation promoted by UV irradiation over Ni/TiO_2. Applied Catalysis B: Environmental, 2015, 168–169: 416–422
64. Hoch L B, Wood T E, O'Brien P G, Liao K, Reyes L M, Mims C A, Ozin G A. The rational design of a single-component photocatalyst for gas-phase CO_2 reduction using both UV and visible light. Advancement of Science, 2014, 1(1): 1400013
65. Ghuman K K, Wood T E, Hoch L B, Mims C A, Ozin G A, Singh C V. Illuminating CO_2 reduction on frustrated Lewis pair surfaces: investigating the role of surface hydroxides and oxygen vacancies on nanocrystalline $In_2O_{3-x}(OH)y$. Physical Chemistry Chemical Physics, 2015, 17(22): 14623–14635
66. Hoch L B, O'Brien P G, Jelle A, Sandhel A, Perovic D D, Mims C A, Ozin G A. Nanostructured indium oxide coated silicon nanowire arrays: a hybrid photothermal/photochemical approach to solar fuels. ACS Nano, 2016, 10(9): 9017–9025
67. Jia J, O'Brien P G, He L, Qiao Q, Fei T, Reyes L M, Burrow T E, Dong Y, Liao K, Varela M, Pennycook S J, Hmadeh M, Helmy A S, Kherani N P, Perovic D D, Ozin G A. Visible and near-infrared photothermal catalyzed hydrogenation of gaseous CO_2 over nanostructured $Pd@Nb_2O_5$. Advanced Science, 2016, 3(10): 1600189
68. Upadhye A A, Ro I, Zeng X, Kim H J, Tejedor I, Anderson M A, Dumesic J A, Huber G W. Plasmon-enhanced reverse water gas shift reaction over oxide supported Au catalysts. Catalysis Science & Technology, 2015, 5(5): 2590–2601
69. Tahir M, Amin N S. Performance analysis of nanostructured NiO-In_2O_3/TiO_2 catalyst for CO_2 photoreduction with H_2 in a monolith photoreactor. Chemical Engineering Journal, 2016, 285: 635–649
70. O'Brien P G, Sandhel A, Wood T E, Jelle A A, Hoch L B, Perovic D D, Mims C A, Ozin G A. Photomethanation of gaseous CO_2 over Ru/silicon nanowire catalysts with visible and near-infrared photons. Advanced Science, 2014, 1(1): 1400001
71. Hisatomi T, Maeda K, Takanabe K, Kubota J, Domen K. Aspects of the water splitting mechanism on $(Ga_{1-x}Zn_x)(N_{1-x}O_x)$ photocatalyst modified with $Rh_{2-y}CryO_3$ cocatalyst. Journal of Physical Chemistry C, 2009, 113(51): 21458–21466
72. Hisatomi T, Miyazaki K, Takanabe K, Maeda K, Kubota J, Sakata Y, Domen K. Isotopic and kinetic assessment of photocatalytic water splitting on Zn-added Ga_2O_3 photocatalyst loaded with $Rh_{2-y}CryO_3$ cocatalyst. Chemical Physics Letters, 2010, 486(4–6): 144–146
73. Hou X, Hou H J M. Roles of manganese in photosystem II dynamics to irradiations and temperatures. Frontiers in Biology, 2013, 8(3): 312–322
74. Zhang F, Cady C W, Brudvig G W, Hou H J M. Thermal stability of $[Mn(III)(O)_2Mn(IV)(H_2O)_2(Terpy)_2](NO_3)_3$ (Terpy = 2,2′:6′,2″-terpyridine) in aqueous solution. Inorganica Chimica Acta, 2011, 366 (1): 128–133
75. Hou H J M. Hydrogen energy production using manganese/semiconductor system inspired by photosynthesis. International Journal of Hydrogen Energy, 2017, 42(12): 8530–8538
76. Wang L, Wang Y, Cheng Y, Liu Z, Guo Q, Ha M N, Zhao Z. Hydrogen-treated mesoporous WO_3 as a reducing agent of CO_2 to fuels (CH_4 and CH_3OH) with enhanced photothermal catalytic performance. Journal of Materials Chemistry. A, Materials for Energy and Sustainability, 2016, 4(14): 5314–5322
77. Zheng Z J, He Y, He Y L, Wang K. Numerical optimization of catalyst configurations in a solar parabolic trough receiver-reactor with non-uniform heat flux. Solar Energy, 2015, 122: 113–125
78. Han S, Chen Y, Abanades S, Zhang Z. Improving photoreduction of CO_2 with water to CH_4 in a novel concentrated solar reactor. Journal of Energy Chemistry, 2017, 26(4): 743–749
79. Chanmanee W, Islam M F, Dennis B H, MacDonnell F M. Solar photothermochemical alkane reverse combustion. Proceedings of the National Academy of Sciences of the United States of America, 2016, 113(10): 2579–2584
80. T-Raissi A, Muradov N, Huang C, Adebiyi O. Hydrogen from solar via light-assisted high-temperature water splitting cycles. Journal of Solar Energy Engineering, Transactions of the ASME, 2007, 129 (2):184–189
81. Docao S, Koirala A R, Kim M G, Hwang I C, Song M K, Yoon K B. Solar photochemical-thermal water splitting at 140°C with Cu-loaded TiO_2. Energy & Environmental Science, 2017, 10(2): 628–640
82. Schwartzenberg K C, Hamilton J W J, Lucid A K, Weitz E, Notestein J, Nolan M, Byrne J A, Gray K A. Multifunctional photo/thermal catalysts for the reduction of carbon dioxide. Catalysis Today, 2017, 280(Part 1): 65–73